scientific reports

Check for updates

OPEN

Constraining the impact of chlorine as a neutron absorber in next-gen fast reactor designs

K. Hanselman[1]✉, I. J. Allan[1,2], S. A. Kuvin[1], T. Kawano[1], N. Kleedtke[1], H. Y. Lee[1], S. N. Paneru[1], N. Thompson[1], J. Winkelbauer[1], T. Cisneros[3], B. Harper[3] & M. Wargon[3]

The role of chlorine as a neutron poison and as a seed for producing radioactive waste in nuclear systems has driven a renewed interest to improve its nuclear data uncertainties. Additionally, basic and applied science programs that use CLYC (Cs_2LiYCl_6:Ce) detectors for neutron spectroscopy and monitoring are also very sensitive to any change in chlorine nuclear data for simulations of the detector response. In this work, sensitivities relevant for these different applications are addressed through simulations of the efficiency of CLYC detectors in a fast fission spectrum when applying new chlorine nuclear data as input. These simulations are validated by an experimental measurement using CLYC detectors coupled to an ionization chamber loaded with a ^{252}Cf spontaneous fission source. The results are then used to obtain the first reliable direct measurement of the ^{35}Cl(n,p_0) and summed ^{35}Cl(n,p+n,α) fission spectrum average cross sections, found to be 54.7(32) and 105.0(98) mb, respectively. The results are within uncertainty of calculated fission spectrum averaged cross sections based on recently re-evaluated chlorine nuclear data, which confirm recent impact studies performed for the Molten Chloride Reactor Experiment. Meanwhile, there currently exists only one published criticality benchmark experiment that is sufficiently sensitive to chlorine nuclear data. Discrepancies are found with this set of criticality safety benchmarks, which are more sensitive to thermal and epithermal neutron energies than the energies, above 100 keV, tested in this current work. Hence, there is still a need to re-evaluate the chlorine nuclear data at lower energies to assess these discrepancies. Interpretation of the data from future "faster" criticality benchmarks, which are needed for next-gen fast reactor designs, benefit from the improved constraints on the chlorine nuclear data validated in this work.

In nuclear environments consisting of chloride salts, chlorine plays a significant role, both as a neutron poison affecting simulations of criticality coefficients and as a seed for producing radioactive waste. In systems with a thermalized ("room temperature") neutron spectrum, the dominant neutron absorption reaction on ^{nat}Cl is neutron capture (n,γ) on ^{35}Cl, producing long-lived ^{36}Cl with a half-life of about 300,000 years. As the average neutron energy increases above 100 keV, the ^{35}Cl(n,p)^{35}S reaction plays a more important role than (n,γ) and also produces shorter-lived ^{35}S ($T_{1/2}$ = 87.4 days). However, until recently the cross section for this channel in this energy range was poorly known and unconstrained by any experimental measurements. For next-gen reactor designs like the Molten Chloride Fast Reactor (MCFR), which uses liquid salts as both a coolant and fuel, the lack of precision in the understanding of chlorine as a neutron poison has led industry nuclear data users to request new nuclear data measurements and evaluations [1], with much of the momentum being driven by companies such as TerraPower, Moltex, and Core Power. TerraPower (TP) is currently leading the Molten Chloride Reactor Experiment (MCRE), a collaboration with Idaho National Laboratory under the investment of the U.S. Department of Energy which serves as a validation experiment prior to development of a commercial MCFR. Beyond the fast reactor application, improving the fidelity of chlorine nuclear data is also driven to improve criticality safety analyses, including for aqueous chloride operations at LANL [2].

Recently, the knowledge surrounding neutron-induced reactions on chlorine at fast neutron energies was improved through new differential measurements on ^{35}Cl [3], the most naturally abundant isotope. These measurements and others cited within supported a re-evaluation of chlorine nuclear data to create new ENDF6-formatted files that are used to generate inputs for particle transport codes such as MCNP6.3 [4] and GEANT4 [5–7]. The impact of the recently updated chlorine evaluation, labeled LANL-TP in Ref. [3] and in this work, was assessed in the context of the MCRE in Ref. [8]. In particular, the new evaluation reduces the magnitude of the ^{35}Cl(n,p) cross

[1]Los Alamos National Laboratory, Los Alamos 87545, NM, USA. [2]North Carolina State University, Raleigh 27695, NC, USA. [3]TerraPower LLC, Bellevue 98008, WA, USA. ✉email: khanselman@lanl.gov

section by a significant factor (∼50% in the fast-energy range), reducing its neutron absorption, and provides better constraints on the previously large (or undefined) uncertainties that, in turn, led to large uncertainties in reactivity calculations of the MCRE. However, additional differential and integral measurements would support further fine-tuning of the evaluation and further reduce uncertainties. Integral criticality benchmark measurements are currently being developed with sensitivities that are tuned to match the applications. However, as discussed in "Impact of updated chlorine nuclear data", the only criticality benchmark sufficiently sensitive to chlorine nuclear data that is currently available in the International Criticality Safety Benchmark Evaluation Project (ICSBEP) handbook was designed to be mostly sensitive to thermal and epithermal neutrons.

In this work, we report on an effort to validate available chlorine nuclear data evaluations in a configuration that is uniquely sensitive to fast neutrons in a fast fission spectrum. This was accomplished by coupling two types of chlorine-dependent scintillation detectors, ^{6}Li-depleted CLYC (utilizing a cylindrical elpasolite crystal $Cs_2{}^{7}LiYCl_6$:Ce, hereafter referred to as "C7LYC") and ^{6}Li-enriched CLYC ("C6LYC"), to an ionization chamber loaded with a ^{252}Cf spontaneous fission source. These types of detectors are now commonly used in modern academic studies and direct applications [9–11], including the CoGNAC array at LANSCE [12,13], from which spare detectors were used in this study. Many of the recent measurements of ^{35}Cl(n,p) influencing the new evaluation have also been performed using CLYC detectors (see Ref. [3] for a summary).

Because of their larger cross sections at these energies, the reactions that dominate the neutron-specific signals in the C7LYC crystal are expected to come from neutron-induced reactions on ^{35}Cl, with approximately 5% of the measured yield coming from reactions on other nuclei. The observed spectra of detector events are compared to simulations of the experimental setup using both MCNP6.3 [4] and GEANT4.11.2 [5–7] under variations of the nuclear data input libraries, then used in a forward-propagation approach to extract experimental fission spectrum average cross sections (SACS). The SACS can be calculated from the energy dependent cross section, $\sigma(E)$, after being weighted by a distribution of incident neutrons $\rho(E)$, as given by:

$$\sigma^{\mathrm{SACS}} = \frac{\int \sigma(E)\rho(E)dE}{\int \rho(E)dE}. \tag{1}$$

In Table 1, this equation is used to calculate the fission spectrum average cross sections from different evaluations by integrating the ^{252}Cf spontaneous fission (s.f.) neutron spectrum as evaluated by Mannhart [14], in both tabulated and parameterized forms, with different energy-dependent chlorine cross sections. The cross sections chosen were ^{35}Cl(n,p_0)$^{35}S_{g.s.}$, populating only the ground state of ^{35}S, and the summed ^{35}Cl(n,p+n,α), as these were the two channels able to be discriminated by the detectors used in this work. Figure 1 illustrates the overlap between the Mannhart-evaluated ^{252}Cf(s.f.) spectrum and several evaluations of the ^{35}Cl(n,p_0) cross section, including LANL-TP. The current chlorine evaluation in ENDF/B-VIII.1 is identical to ENDF/B-VIII.0 (2018) but has had only minor updates since ENDF/B-VII.1 (2007). Meanwhile, the current LANL-TP data could be considered as a candidate for the next ENDF/B-IX release after sufficient validation. Based on these calculations, one can predict that a C7LYC detector would observe approximately 40% fewer (n,p_0) events using the LANL-TP evaluation than would be predicted by ENDF/B-VIII.1, under a first-order assumption that each chlorine atom in the CLYC crystal sees the unperturbed neutron spectrum from the initial spontaneous fission. However, neutrons will undergo absorption and scattering in surrounding materials, as well as with the other atoms in the CLYC itself such that the average neutron spectrum will be different and a correction factor needs to be applied to the term ρ(E) in Eq. 1. To quantify this, we rely on the simulations using the particle transport codes MCNP6.3 and GEANT4.11.2, discussed in the following two sections. With this forward propagation approach, Eq. 1 is modified to be:

$$\sigma^{\mathrm{SACS}}_{\mathrm{exp}} = \sigma^{\mathrm{SACS}}_{\mathrm{calc}} \times \frac{\mathrm{N}^{n,*}_{\mathrm{exp}}}{\mathrm{N}^{n,*}_{\mathrm{sim}}} \times \frac{\mathrm{N}^{\mathrm{neutrons}}_{\mathrm{sim}}}{\mathrm{N}^{\mathrm{fission}}_{\mathrm{exp}} \times \overline{\nu}} \tag{2}$$

where $\sigma^{\mathrm{SACS}}_{\mathrm{calc}}$ is the calculated SACS from Table 1, for which the same neutron source shape is used as an input in the simulations. $\mathrm{N}^{n,*}$ are the number of counts associated with each reaction channel, (n, p_0) or $(n, p) + (n, \alpha)$, for both the measurement and simulations; $\mathrm{N}^{\mathrm{fission}}_{\mathrm{exp}}$ is the number of fission counts measured by the ionization

Calculated ^{252}Cf(s.f.) SACS (mb)				
	^{35}Cl(n,p_0)		^{35}Cl(n,$p+n$, α)	
(n,X) file	Tabulated	Watt	Tabulated	Watt
ENDF/B-VIII.1	82.0(96)	81.3(96)	138.6(311)	138.3(312)
JENDL-5	50.9(58)	50.5(57)	101.0(215)	101.0(217)
LANL-TP	54.2(22)	53.8(23)	103.5(135)	103.5(139)

Table 1. Calculated SACS for ^{35}Cl(n,p_0) and ^{35}Cl(n,$p + n, \alpha$) using different evaluated cross sections and neutron spectra. The neutron spectrum is based on the Mannhart evaluation, as either the Watt parameterization (a = 1.209(15) MeV, b = 0.836(107) MeV^{-1}) [14], or "tabulated", as included in the ENDF/B library. Uncertainties were estimated by Monte Carlo sampling the evaluated cross section and spectrum covariances; the lack of fast-energy covariance information in the ENDF/B-VIII.1 and JENDL-5 files was compensated using covariances from TENDL-2023 [15].

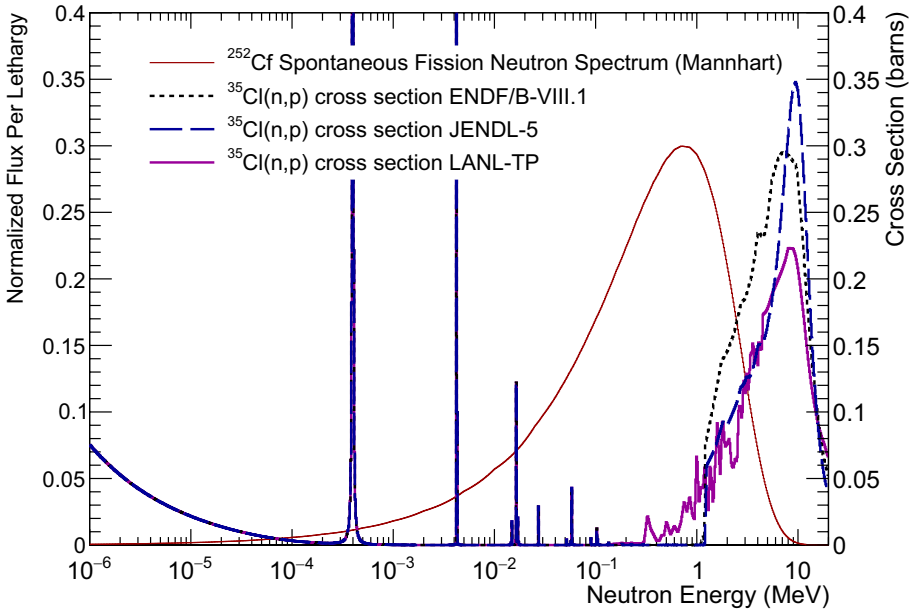

Fig. 1. The outgoing neutron spectrum from a spontaneous fission ^{252}Cf source is compared to the ^{35}Cl(n,p) cross sections of interest in this work, on a relative scale. This cross section was significantly decreased in Ref. [3] relative to ENDF/B-VIII.1 in the overlapping region with the s.f. neutron field, between ≈1 to 6 MeV.

chamber; and $N_{sim}^{neutrons}$ is the number of neutron events or histories input into the simulation, converted to fission counts by $\overline{\nu}$, the expected neutron multiplicity per fission event.

"Methods" provides a description of the experimental setup, analysis methods, and simulations. In "Results", a forward-propagation technique is employed to benchmark different evaluations against each other by comparing the calculated to experimental yields, which also allows for the ^{252}Cf spontaneous fission spectrum average cross section to be determined for the ^{35}Cl(n,p_0) and ^{35}Cl(n,p + n, α) reactions. The impact of the results of this work are discussed in "Impact of updated chlorine nuclear data", where potential discrepancies in the neutron capture rate at thermal energies serve to motivate further improvements that are needed on the evaluated chlorine nuclear data inputs. These improvements are necessary for criticality safety applications, for which nuclear data are to be benchmarked against integral experiments such as the Chlorine Worth Study [16] (CWS) and the recently completed TEX-Cl experiments [17].

Methods

Measurement

The experimental setup was constructed at the Weapons Neutron Research (WNR) facility of the Los Alamos Neutron Science Center (LANSCE). Each CLYC detector was placed 88.5(2) cm away from a ^{252}Cf spontaneous fission source, measured from face to face of the detector housing and fission chamber with the aid of laser guides. This flight path length represented a good optimization between timing resolution and solid angle for counting statistics, and was remeasured before and after each configuration change. Two different CLYC detectors were used independently, one depleted in ^{6}Li ("C7LYC") and one enriched ("C6LYC"). While the C7LYC was the chief instrument for extracting mostly background-free reactions on ^{35}Cl, the ^{6}Li(n,t) reaction in the C6LYC was desired as a reference and for quantification of "room return" neutrons. The CLYC crystals within each detector were listed to have nominal 1.5"×1.5" cylindrical dimensions; however, CT scans revealed the C7LYC to have a smaller than expected diameter of 1.35". The source was a cylindrical ion chamber which allowed for self-counting of fission events and timing coincidences with external detectors. The ionization chamber provided a trigger and "zero-time" for all fission events and therefore a reference to normalize the neutron interactions observed in the CLYC per fission event. The fissionable material was deposited on a 1 cm-diameter surface of a radius R ≃ 9.3 mm steel hemisphere inside a 2.54 cm×6.57 cm cylindrical steel housing. Further details of the source and its implementation in MCNP can be found in Ref. [18]. To minimize neutron scattering backgrounds, both the source and the detectors were mounted on thin steel rails attached to aluminum stands, the effects of which were studied for uncertainty quantification discussed later. The measurements were also performed above a solid concrete floor and next to two concrete shielding walls, about 93.7(2) cm above the floor and more than a meter away from either shielding wall. A photograph of the setup and its implementation in MCNP6.3 are shown in Fig. 2. Visible in the photograph is a stilbene detector at the mirror angle relative to the source, run in parallel for a separate characterization study; its effect on room background was negligible and therefore not simulated.

There were two main geometrical configurations, varying the source-detector angle between 0° and 45° while maintaining all relative distances. This was to have a consistency check against the presumed isotropy of the source neutron spectrum. Additional details about the ionization chamber containing the ^{252}Cf source

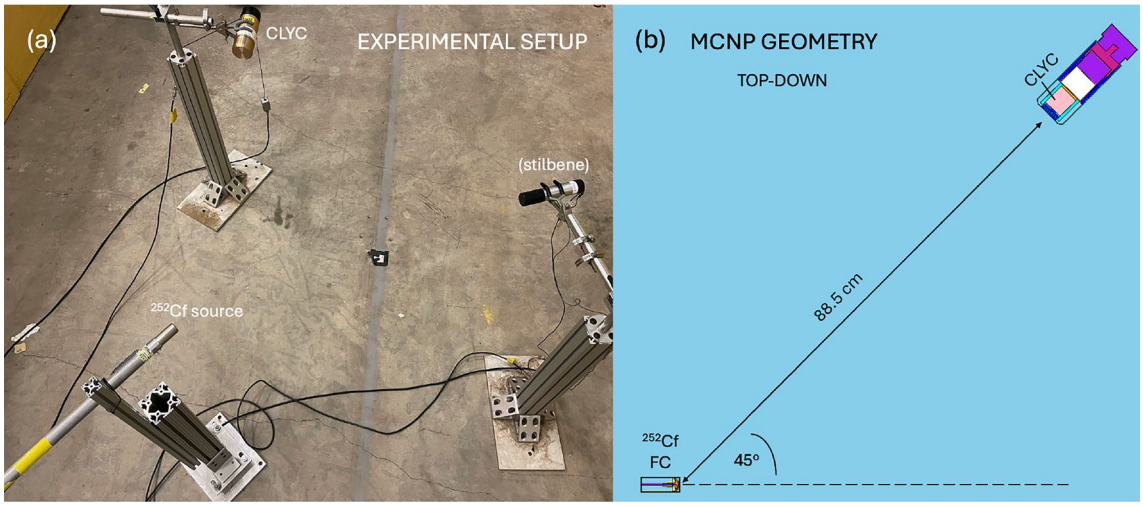

Fig. 2. The experimental setup, (**a**) as photographed in 15R for the 45° configuration and (**b**) as implemented in MCNP6.3. In (**a**), the ^{252}Cf(s.f.) source is at the bottom-left while the CLYC detectors were positioned at the top. For simplicity, the stilbene detector seen at the mirror 45° position is not shown in the MCNP representation. Also not shown in (**b**) are the concrete floor and flight path walls, which were included in the calculations as sources of room-return background (photographed by author S.A.K.).

can be obtained from Ref. [18], which employed a similar setup as this work but was focused on extracting ^{6}Li differential cross sections. This work instead focuses on integral spectrum-averaged quantities to limit the uncertainties associated with extracting the neutron energy via time-of-flight, but still relies on the timing to discriminate between different reaction components. In addition, a timing cut is applied to limit contributions from downscatter. The signals from the ionization chamber and CLYC detector were read out using 500 MS/s sampling digitizers from CAEN, with waveforms digitized for offline analysis to optimize neutron pulse shape discrimination and to correct for timing amplitude-risetime-walk effects. The fission rate was found to be consistent with that measured by Ref. [18], accounting for decay in the intervening years and potential isotopic contamination due primarily to ^{250}Cf and ^{248}Cm. Extrapolations using previously reported assay values [18] estimate the uncertainty contribution to the fission rate due to such contamination at the sub-percent level for this work's purposes.

Analysis and data reduction

The energy calibration (in electron-equivalent "MeVee") of the CLYC detector signals was performed using multiple γ-emitting sources, namely ^{57,60}Co, ^{137}Cs, ^{88}Y, and ^{22}Na. The prompt coincidences between the ionization chamber (zero-time) and the arrival of the fission γ-rays to the CLYC detector were used to calibrate the relative timing for the incident neutrons. Discrimination between neutron and γ-ray signals in the CLYC was made possible by pulse-shape discrimination (PSD), as shown in Fig. 3a, c. Here the PSD variable was defined as the difference between long- and short-gate integrals of the recorded waveforms in ratio with the long-gate integral. This allowed for clear distinction between incident neutrons and γ-rays for the majority of energies.

With neutron-only events selected, the kinematic correlations between detected energy versus time difference with the source (related to the incident neutron energy) can be observed, as shown in Fig. 3b, d. These correlations are used to identify the relative contributions due to different reactions such as ^{35}Cl(n,p_0), ^{35}Cl(n,$p_{x>0}+n,\alpha$), and ^{7}Li(n,nt+α) in the C7LYC detector. For the C6LYC detector, additional contributions due to ^{6}Li(n,t) and ^{6}Li(n,nd+α) are observed, including timing "wraparound" bands of low-energy and thermalized neutrons which are slow enough to fall into the next events' timing windows. Finally, by dividing the number of observed events within a particular kinematic gate by the total number of corresponding source fissions, the integrated number of counts for (n,p_0) and (n,p+n,α) per reference fission event could be measured, which are given in Table 2. Contributions to the source chamber signals from the dominant alpha decay channel were eliminated by online waveform filtering.

If PSD capabilities were improved such that proton recoil events could be discriminated, with good figure-of-merit, from alpha recoil events above 1 MeVee threshold, it would be feasible to extract the (n,p) and (n,α) yields independently. Here, the threshold for separating (n,p) and (n,α) events are at approximately 3 MeVee, therefore we report the combined (n,p+n,α) yields instead. In addition, the contributions due to ^{7}Li(n,nt+α) and ^{6}Li(n,nd+α) need to be subtracted to obtain the ^{35}Cl(n,p+n,α) counts, based on the simulated yields. This contribution from lithium breakup is approximately 4% for C7LYC, as discussed in "Background due to lithium breakup". However, due to larger uncertainties associated with the ^{6}Li(n,nd+α) reaction, we report only the ^{35}Cl(n,p_0) yield from the C6LYC.

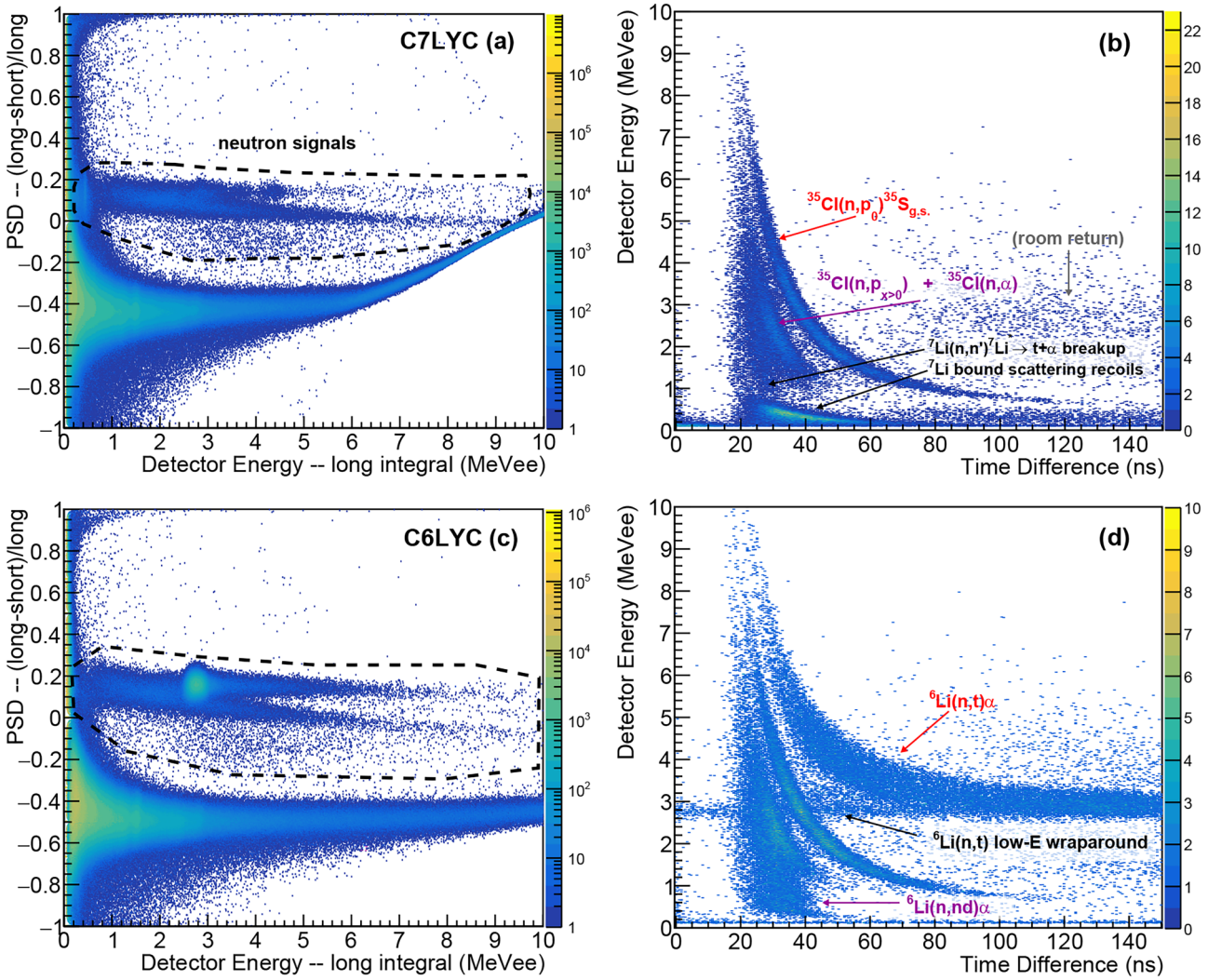

Fig. 3. Sample analysis plots for the two detectors: (**a**) PSD for C7LYC, showing the cut made to isolate primarily neutron-induced events; (**b**) C7LYC kinematics associated with the PSD cut, shown as signal energy versus time difference with the prompt γ-rays from the source. (**c,d**) Analogous plots for the C6LYC. The signal energy has been calibrated using several well-known gamma sources (see text). The z-axes are number of raw counts per bin.

MCNP and GEANT4 simulations

The experimental setup described in "Measurement" was modeled in both MCNP6.3 and GEANT4.11.2, an example of which is shown in Fig. 2b. The use of both codes allowed for independent comparisons of the data under different modeling mechanisms and assumptions, especially since both codes use as input different processed formats of the data. The MCNP ACE file inputs that are derived from the ENDF6 formatted nuclear data libraries were produced in-house using NJOY [20]. For GEANT4, the LANL-TP ENDF6 file was processed into a G4NDL input file with help from the GEANT4 developers at CIEMAT [21], which was then benchmarked against the NDL files that are publicly distributed for ENDF/B-VIII.0 on the IAEA website (https://www-nds.iaea.org). The "Shielding" physics list, which instantiates the "High Precision Neutron Model" required to utilize the G4NDL files, was employed for the GEANT4 calculations in this work. For both GEANT4 and MCNP simulations, the ENDF/B-VIII.0 evaluation is adopted as a base for all nuclei but comparisons are made by whether the LANL-TP or the unchanged ENDF/B-VIII.0 chlorine files are used. In GEANT4, tests were also performed using JENDL-4.0u as the base input library (JENDL-5.0 is not yet publicly available) for checking any nuclear data sensitivities to scattering off surrounding materials. However, in the following, we focus on results using LANL-TP to those using the base ENDF/B-VIII.0, as a goal would be for the updated fast evaluation in LANL-TP to be adopted in future releases of ENDF/B.

Neutron source

For the MCNP simulation, the (presumed uniform) deposition of the source material within the chamber was treated using a source defined on the surface of the inner steel button, starting on-axis and extending backward to

		Detector	Counts per fission (10^{-6})	
Configuration	$N_{fissions}$	Radius (mm)	$^{35}Cl(n,p_0)$	$^{35}Cl(n,p+n,\alpha)$
A) C7LYC at 45° (I)	1.628×10^{10}	17.1	1.006(22)	1.876(22)
B) C7LYC at 45° (II)	1.073×10^{10}	17.1	1.001(22)	1.877(23)
C) C7LYC at 0°	1.983×10^{10}	17.1	1.042(22)	1.972(23)
D) C6LYC at 45°	1.157×10^{10}	19.1	1.239(28)	
E) C6LYC at 0°	0.845×10^{10}	19.1	1.280(27)	

Table 2. The number of fissions per experimental run configuration were obtained from the total number of signals detected in the fission chamber. Signals from α-decay (the dominant decay process by ~97% [19]) were cut out by online waveform filtering. The two C7LYC runs at 45° are treated as independent due to the amount of time and reconfiguration between them. The presented uncertainties are primarily statistical, taking into account background subtraction of the ^{6}Li(n,t) wraparound for the C6LYC runs, plus an additional 2% systematic uncertainty for (n,p_0) due to the graphical cut. For the ^{35}Cl(n,p + n,α), a 1% additional uncertainty is adopted due to the subtraction of (n,$n't$+α) reactions from the C7LYC.

Dominant systematic uncertainties	
% Value	Source
2.0	Graphical cuts
4.0	Source anisotropy
3.1	Efficiency (C7 p_0)
3.6	Efficiency (C7 p+α)
1.7	Efficiency (C6 p_0)
1.0	^{7}Li inelastic breakup subtraction (C7 p+α)
2.0	General scattering material

Table 3. Listed are the dominant sources of systematic uncertainty found throughout the study. Values have been calculated or estimated based on the methods described in the text.

a diameter of 1 cm. In GEANT4, a similar geometry was defined using the G4 "General Particle Source" routines, defined along the surface of the partial sphere. The source was then allowed to emit neutrons isotropically in solid angle with an energy distribution determined by the Watt parametrization in the MCNP simulation and by a tabulated distribution in the GEANT simulation, both derived from the evaluation by Mannhart [14]. The simulation was executed in two modes: (1) isotropic in all directions to simulate the effect of room return background from the surrounding floor and walls or (2) assumed isotropic but biased in a cone in the direction of the CLYC detector.

Geometry

The $Cs_2{}^{7,6}LiYCl_6$ crystal was a custom mixture of its primary components, using atomic fractions, natural chlorine, and 100% enrichment of the lithium in either ^{7}Li or ^{6}Li. The effect of lithium enrichment on the simulated yield due to chlorine-induced reactions was found to be insignificant. The simulations can then be corrected for the actual lithium enrichment of the C6LYC which was 95% ^{6}Li, but above 99% ^{7}Li for the C7LYC. Being a small fraction of the total mass, the Ce doping was neglected in the material definition. The density of the crystal was set to the manufacturer's value of 3.31 g/cm^3. Directly in front of the CLYC crystal is a mixture of aluminum casings and neoprene padding, therefore the uncertainties due to neutron absorption prior to interacting with the CLYC crystal were estimated by varying the thicknesses and density of these materials. Perturbations to the size and location of the crystal were used to estimate the uncertainty of the detector geometric efficiency.

In addition to the fission source and detector, the walls and floor of the flight path were included in the model and assigned concrete as their material (the Los Alamos (MCNP) Mix listed in Ref. [22]). The floor was about 93.7 cm from the mid-plane of the source, while the shielding walls, each at a slight angle relative to the source axis, only approached the CLYC detector at a nearest distance of ~1.4 m. In the primary simulations, the detector stand components, consisting of 80/20 aluminum stands and thin steel rods, were initially neglected for simplicity. These smaller components were later added back in after slight systematic offsets were observed in the subsequent C/E (calculated-over-experimental) values. A flat +2% correction to the main production runs for all configurations was decided on after studying the extra background introduced by these components. The uncertainty due to this correction is included in the "general scattering material" term of Table 3 further discussed in "Uncertainty quantification".

Furthermore, through CT scanning performed locally at LANL, the C7LYC was found to have a cross sectional diameter of 1.35" rather than the expected (and simulated) 1.50". Additional simulations were then

	LANL-TP				ENDF/B-VIII.0			
	^{35}Cl(n,p_0)		^{35}Cl(n,$p+n$,α)		^{35}Cl(n,p_0)		^{35}Cl(n,$p+n$,α)	
Config.	GEANT4	MCNP	GEANT4	MCNP	GEANT4	MCNP	GEANT4	MCNP
A	1.002(63)	0.990(66)	1.001(59)	1.000(61)	1.450(87)	1.526(100)	1.306(74)	1.386(85)
B	1.007(63)	0.995(67)	1.000(59)	1.000(62)	1.454(88)	1.533(101)	1.306(72)	1.386(85)
C	0.967(60)	0.956(64)	0.952(54)	0.952(58)	1.396(84)	1.472(96)	1.244(69)	1.319(81)
D	1.026(65)	1.000(61)			1.481(88)	1.577(94)		
E	0.993(61)	0.966(59)			1.429(84)	1.524(91)		

Table 4. C/E (calculated-over-experimental) values for the various simulated configurations, relative to the experimental values in Table 2. As discussed in the text, C6LYC values for ^{35}Cl(n, p+n, α) have been neglected due to complications from ^{6}Li(n,nd) contamination. Uncertainties are 1σ values and include both statistical and systematic contributions.

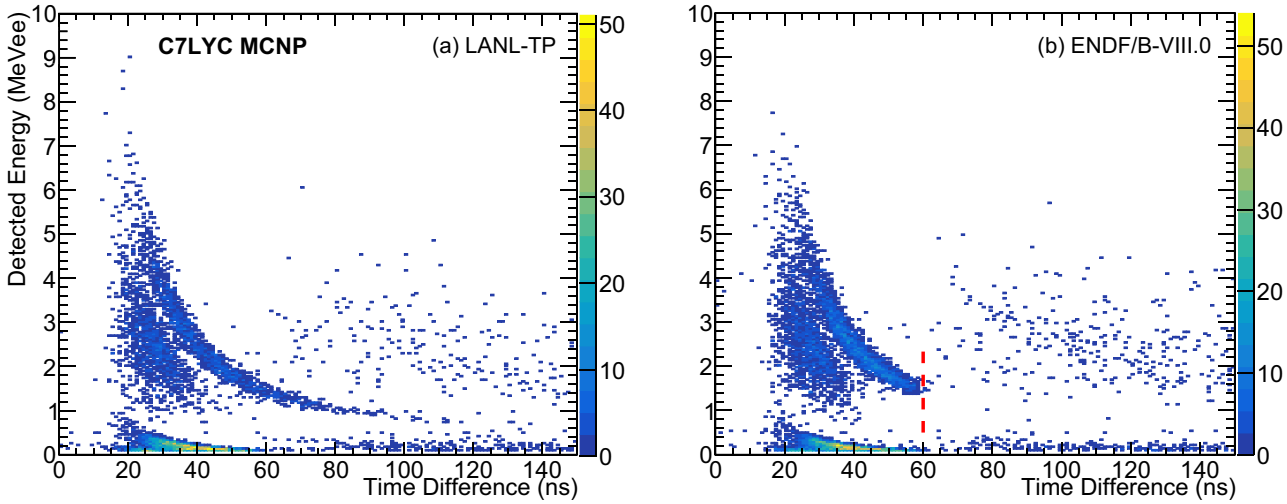

Fig. 4. Example kinematic plots of MCNP-simulated interactions in the C7LYC crystal from an isotropic ^{252}Cf source. (**a**) Uses the LANL-TP evaluation for ^{35}Cl while (**b**) shows the result for ENDF/B-VIII.0; the files of all other isotopes were kept as ENDF/B-VIII.0. The neutron timing corresponding to the 1.2 MeV drop-off in the ENDF/B-VIII.0 file, below which the cross section becomes artificially negligible, has been highlighted with a dotted red line. Z-axes are again counts per bin.

carried out, which confirm that the expected difference is dominated by the difference in solid angle coverage, resulting in a correction factor of $(1.35)^2/(1.50)^2 = 0.81$ that was applied to the simulated yields generating the C/E values of Table 4 for the C7LYC. This correction was also taken into account through the systematic uncertainty tabulated later in Table 3.

Post processing

For particle-tracking analysis in MCNP, the PTRAC functionality was used with the HDF5 output made available in MCNP6.3. For testing and verification purposes, full event histories were written from creation to termination to characterize scattering from background contributors that influence detections in the crystal. However, for the full quantitative analysis runs, cell filtering was applied so that only events taking place in the CLYC crystal were written, to cut down on data storage and analysis time.

Example simulated energy-versus-timing plots are given in Figure 4, using both LANL-TP and ENDF/B-VIII.0 for ^{35}Cl. All other isotopes were kept as ENDF/B-VIII.0. The detected energy was calibrated from MeV to MeVee by taking quenching factors from the literature [10,11] and adjusting manually until the simulated signals matched those measured. Then similar kinematic cuts as applied to the measured data could be used to calculate equivalent counts-per-fission quantities for comparison, after correcting the number of neutron histories by the 3.76 average number of neutrons ($\bar{\nu}$) from spontaneous fission [18].

The neutron timing corresponding to the 1.2 MeV drop-off in ENDF/B-VIII.0, where the evaluation produces negligible cross-section shown in previous works to be unphysical [3], has been highlighted by a dotted red line. These plots, being isotropic in neutron emission from the source, are meant to demonstrate the reproduction of related backgrounds like the room-return from concrete. Similar calculations were made for other configurations as well, including high-statistics runs with a forward-focused source once the background contributions were

characterized. However, one feature, the inelastic breakup of the ^{7}Li highlighted in Fig. 3, is missing from both simulated plots, a discrepancy which is discussed in more detail in the following subsection.

Background due to lithium breakup

The default behavior of the GEANT4 and MCNP simulations do not reproduce the ^{6}Li(n,n')^{6}Li$^{*} \rightarrow d{+}\alpha$ or ^{7}Li(n,n')^{7}Li$^{*} \rightarrow t{+}\alpha$ breakup reactions. This results in a deficiency of simulated events in the region around 1 to 2 MeVee detected energy and 20 to 40 ns in time difference, as observed in the experiment in the right panels of Fig. 3. Similar to the methods used in Ref. [23], these effects can be corrected for manually during the stepping action of the GEANT4 simulation, to reproduce the average energy of the outgoing breakup particles which can then contribute to the the pulse height spectra as expected. This approach cannot be employed in the MCNP simulation, as the necessary correlated outputs are not produced, but could potentially be reconstructed during PTRAC output post-processing from the kinematics of the recoiling neutron. For the purposes of this work, correction factors and uncertainties were taken from the GEANT4 approach and applied to both simulations. A projection of the GEANT4 simulated energy spectrum at relative times between 20 to 40 ns is shown in Fig. 5 that illustrates the expected contributions from lithium breakup. Here, the high energy events due to ^{6}Li(n,t) are excluded such that the difference between the C6LYC and C7LYC spectra shows the relative contribution between the lithium-breakup and the chlorine-induced events. The unscaled C6LYC spectrum is using directly the ENDF/B-VIII.0 inelastic lithium breakup cross sections. The scaled C6LYC spectrum is to highlight the potential nuclear data uncertainty as the ENDF/B-VIII.0 ^{6}Li breakup cross section is systematically larger than the experimental data found in EXFOR, as discussed below. On the other hand, the evaluated ^{7}Li breakup cross section is in better agreement with the experimental data, has a higher threshold, and smaller scale, such that it contributes less uncertainty to the total CLYC spectrum.

For the C7LYC, the contribution due to lithium breakup as a background to the ^{35}Cl($n,p+n,\alpha$) yields is simulated to be 4.1%, which compares to the value of 5% that one obtains simply by calculating the SACS for ^{7}Li($n,nt{+}\alpha$) and ^{35}Cl($n,p+n,\alpha$) and scaling by the stoichiometry (1:6 Li:Cl). A 1% uncertainty on the extracted ^{35}Cl($n,p+n,\alpha$) yield is obtained assuming a 20% uncertainty on the ^{7}Li($n,nt{+}\alpha$) nuclear data. For the C6LYC, however, there are still significant discrepancies between the evaluations of ^{6}Li($n,nd{+}\alpha$) compared to the measured data in EXFOR. As a result, we do not report the ^{35}Cl($n,p+n,\alpha$) yields from the C6LYC, as the subtraction is expected to be a significant correction at the 10% level or more. However, we note that to bring the measured C6LYC yields into agreement with the measured C7LYC yields, we would need to scale the expected(simulated) ^{6}Li($n,nd{+}\alpha$) contribution down by a factor of $\approx$0.65, when using the ENDF/B-VIII.0 library as the input cross section. Qualitatively, this is close to the ratio that ENDF/B-VIII.0 appears to overestimate the reported measurements in EXFOR and the EAF-2010 nuclear data library. Therefore, the C6LYC spectrum may

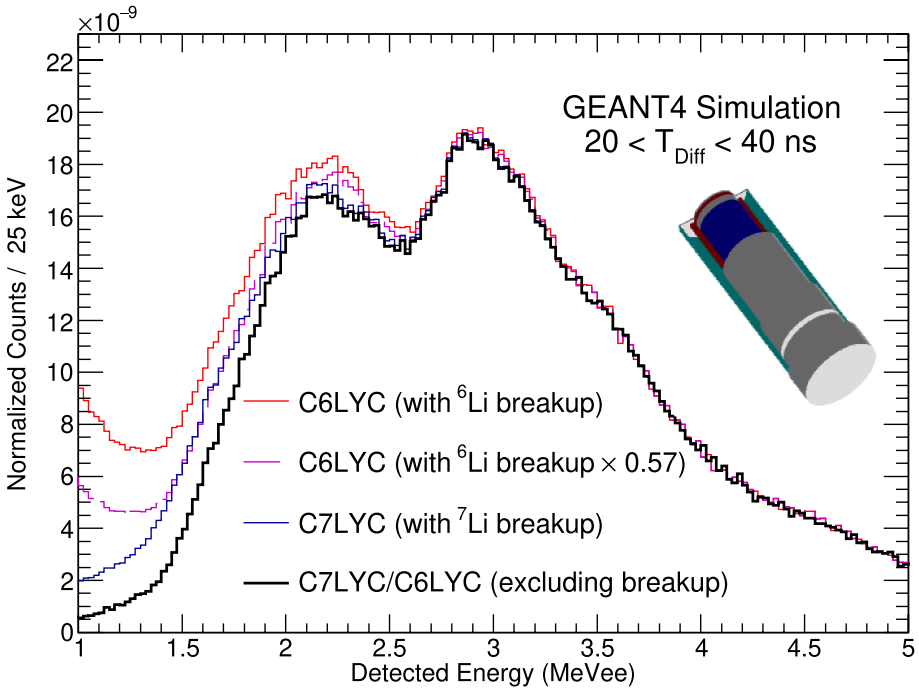

Fig. 5. Difference in GEANT4 simulated energy spectra from the CLYC detector when including or excluding contributions due to ^{6}Li or ^{7}Li breakup reactions (based on ENDF/B-VIII.0 inelastic breakup cross sections). The scaled and unscaled contributions in the C6LYC are intended to reflect potential uncertainty in the evaluated ^{6}Li cross sections. The high energy events from ^{6}Li(n,t) are excluded from this figure. The inset shows the visual representation of the CLYC detector in GEANT4, where the inner (red) and outer (cyan) aluminium shells are cut away to reveal the CLYC crystal (blue).

be re-investigated to validate future improvements to the lithium nuclear data libraries, but is limited to the study of ^{35}Cl(n,p_0) in this work.

Uncertainty quantification

To estimate the net effect of uncertainties in simulated parameters on the final measured quantities, a perturbative first-order analysis was performed on the MCNP description. Key parameters with finite uncertainty known to impact the extracted yields were varied by ±1% and then each run through a full simulated series. The total neutron histories per series (i.e. per perturbation) were 2.5×10^9, and the neutrons were emitted forward in a 5° cone to focus events into the detector. This limited the impact of statistical uncertainty to about 0.2%, giving sensitivity to the systematic scale at ∼0.5% and above.

From these results, a first-order, linear sensitivity matrix was constructed for the integrated yields of ^{35}Cl(n,p_0) and (n,p+n,α), following the method of Ref. [24]. Of the key parameters, five were found to be the most impactful: the CLYC crystal density (1.0%), diameter (0.5/1.5%), and thickness (0.5%), the distance from the source (0.5%), and the a-parameter of the Watt spectrum (1.0%), all listed with their estimated individual uncertainties in parentheses. The double value given for the crystal diameter is the difference between C6LYC/C7LYC driven by the CT scans mentioned above. Other parameters, like the Watt b parameter and the CLYC vertical position, were tested but found not to be sensitive to this level of analysis. With these sensitivities, the total systematic contributions to the integrated yield uncertainties were calculated to be 3.1% for (n,p_0) and 3.6% for (n,p + n,α) in the C7LYC, and 1.7% and 2.3% respectively for the C6LYC, with a high (∼95%) positive correlation. These are included in Table 3 as uncertainties associated with general "efficiencies".

An additional 4% systematic uncertainty was also assigned due to apparent anisotropy in the angular dependence of the incident flux. This was first investigated by comparing the measured source energy spectra both correlated and uncorrelated with events in the CLYC detectors, for both angles. The correlated spectra showed an overall 4% discrepancy in shape with the uncorrelated, leading to the observed discrepancy in central values between configurations A and B with configuration C in Table 2, and similarly between D and E. To characterize this, MCNP simulations were performed in which all major background components, including the aluminum stands and steel rods holding the detectors, were toggled in a systematic way, and their influences on the neutron flux seen by the CLYC detector's space compared. While no significant 0°/45° angle dependence emerged from the scattering background alone, the inclusion of the detector stands was found to contribute an extra +2% yield to the calculated values, the uncertainty of which has been included in Table 3 as "general scattering material". This term also includes more subtle effects more difficult to quantify, such as the precise densities and nuclear data uncertainties of the internal components of the CLYC housing and the surrounding concrete.

Finally, any uncertainty sources that were found to contribute at the sub-percent level, like the uncertainty in $\bar{\nu}$ due to Cf source impurities [18] (∼0.3%), are not shown due to their negligible impact on the total uncertainty at this work's level of precision.

Results and discussion

Given the measured counts-per-fission values reported in Table 2, the corresponding C/E values for various simulated configurations are presented in Table 4 and Fig. 6. Two C7LYC configurations, both at 45°, are treated as independent measurements due to the amount of time and reconfiguration between them. The quoted uncertainties are a combination of statistical and systematic sources from Table 3.

Compared to ENDF/B-VIII.0, the results simulated with the LANL-TP evaluation demonstrate improved agreement with the measurements. C/E values for ^{35}Cl(n,p_0) are within one standard deviation (sigma) of

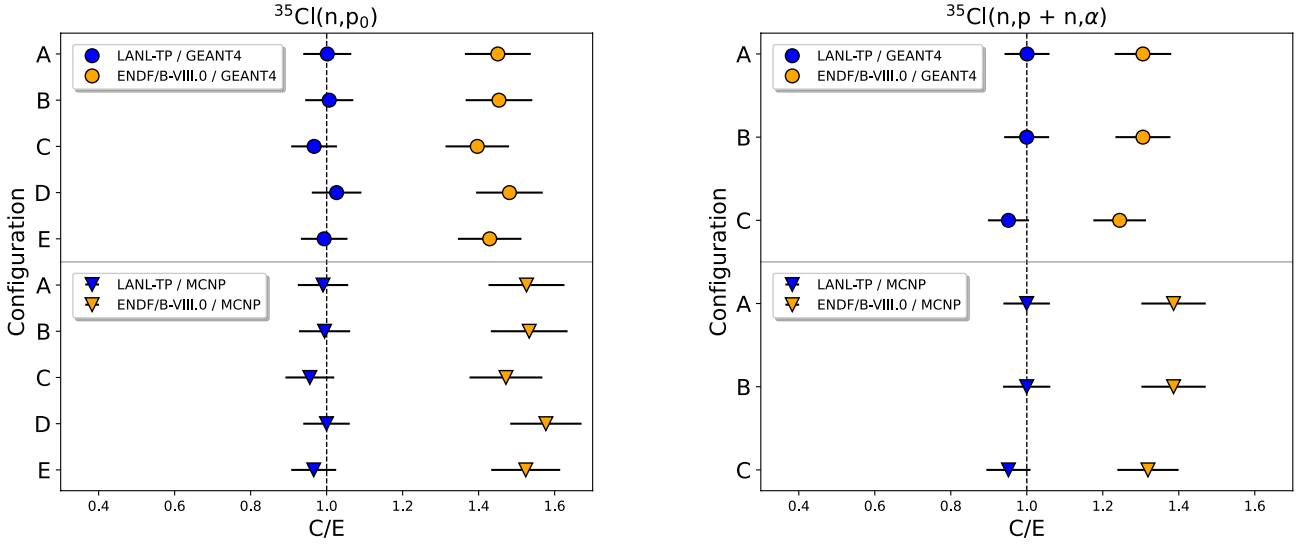

Fig. 6. Visual representation of Table 4.

unity, while those for ENDF/B-VIII.0 are systematically too high by several sigma. This is principally down to the reduction in evaluated cross section above 1.2 MeV mentioned in Ref. [3] driven by the latest cross section measurements. Results for ^{35}Cl(n,p + n,α) follow a similar systematic trend. The general agreement between GEANT4 and MCNP6.3 accounts for potential differences in the treatment of neutron transport between the two codes. When applying the ENDF/B-VIII.0 evaluation as an input, the central values between GEANT4 and MCNP show a slightly larger disagreement compared to LANL-TP, but still within uncertainties. This can be explained by the fact that the abrupt transition of the cross section at 1.2 MeV in the ENDF/B-VIII.0 library is more sensitive to subtle changes in the shape of the neutron flux than the LANL-TP evaluation, which has a smoother transition near the mean of the flux, as illustrated in Figs. 1 and 4.

Given the calculated SACS values in Table 1 and averaged C/E values from Table 4, we have extracted experimentally measured SACS of ^{35}Cl(n,p_0) and ^{35}Cl(n,p + n,α) using both LANL-TP and ENDF/B-VIII.0/1, as well as an uncertainty-weighted average of both. These quantities are presented in Table 5. Up to this point, the ENDF/B-VIII.0 and ENDF/B-VIII.1 labels could be used interchangeably when referring to the chlorine nuclear data as the data was not changed between releases. However, in the following section, comparisons are made with integral benchmark data that are very sensitive to updates, particularly in Pu-239 nuclear data, between the evaluations. Hence, comparisons are made by taking the ENDF/B-VIII.1 evaluation as the base library, and changing whether the LANL-TP chlorine file is included.

Impact of updated chlorine nuclear data

The update of the ^{35}Cl evaluation at fast neutron energies, validated in this work, was initially driven to meet the nuclear data needs for reactor operation for the MCRE. With the net decrease in neutron absorption relative to ENDF/B-VIII.1 at average fission neutron energies, the simulated MCRE performance showed a change in reactivity by approximately 2000 ± 200 pcm [8]. The conclusions in Ref. [8] are reinforced by this current study, as the measured ^{252}Cf fission spectrum averaged chlorine cross sections are consistent within 5-6% of the calculated SACS. The next step for the evaluation is to be benchmarked against integral criticality experiments that are designed to be sufficiently sensitive to chlorine.

As of this writing, the first integral criticality experiment sufficiently sensitive to chlorine nuclear data, the Chlorine Worth Study (CWS), was published in the ICSBEP benchmark handbook [25]. Comprised of stacks of plutonium-based and chlorinated materials, the CWS is most sensitive to ^{239}Pu, ^{35}Cl, and thermal scattering laws, and for chlorine the neutron capture cross section at thermal energies specifically [16]. Still, the true sensitivity at fast neutron energies was unknown because no uncertainty information was available for ^{35,37}Cl(n,X) reactions at average fission neutron energies above 1 MeV, leading either to liberal overestimations or, when "zero" uncertainty was assumed, drastic underestimations. With the updated evaluation of chlorine at fast energies, validated by the CLYC study in this work for fission-typical neutron energies, the sensitivity of the CWS to $^{\mathrm{nat}}$Cl(n,X) reactions at fast energies is now well constrained, thereby allowing focus to be applied to other energy regimes without the risk of compensating error.

A major update to Pu-239 nuclear data, based on a large international collaboration, has been released as part of ENDF/B-VIII.1 that improves performance of simulations of the CWS and multiple other Pu-sensitive criticality benchmarks, compared to the previous ENDF/B-VIII.0. However, discrepancies still exist in the CWS benchmark criticality values when compared to simulations using ENDF/B-VIII.1. The impact of our updated fast evaluation on the CWS is an increase in criticality by ∼100 pcm, moving the simulated values farther outside the 1σ uncertainties of the benchmark values (Figure 7). Here, the difference between the MCRE impact and the CWS impact is that the CWS is much more sensitive to neutron capture on chlorine at thermal energies while the MCRE operation is more sensitive neutron absorption from (n,p) at fast neutron energies. However, the large reduction to neutron absorption at fast neutron energies still leads to a non-negligible change in reactivity for the CWS. With this adjustment, the average 5% to 10% uncertainty in the evaluated (n,p) cross sections at fast energies is not enough to explain the discrepancy in the CWS comparison between simulations and benchmark values.

To investigate potential discrepancies and guide future studies, calculations were performed for the three published cases of the CWS under different percentile perturbations of the LANL-TP ^{35}Cl(n,γ) cross section. This cross section was chosen to represent the impact of chlorine nuclear data below the now well-constrained fast region, in the thermal and epithermal ranges of CWS sensitivity. The adjustments were made to the ACE file directly using the toolkit ACEtk developed by the nuclear data team at LANL, available at https://github.com/njoy/ACEtk, following similar methods to those used in Ref. [24]. CWS calculations using both the perturbed and unperturbed ACE files were then run through MCNP6.3 on LANL's High Performance Computing clusters and the k_{eff} values (neutron multiplicity or reactivity coefficients) compared through C/E analysis.

Extracted experimental SACS (mb)		
Sim. input:	**^{35}Cl(n,p_0)**	**^{35}Cl(n,p + n,α)**
LANL-TP	54.5(38)	105.2(117)
ENDF/B-VIII.0/1	55.0(57)	104.5(177)
Average	54.7(32)	105.0(98)

Table 5. ^{252}Cf(s.f.) SACS for ^{35}Cl cross sections extracted by combining the calculated values in Table 1 with averaged C/E ratios from Table 4.

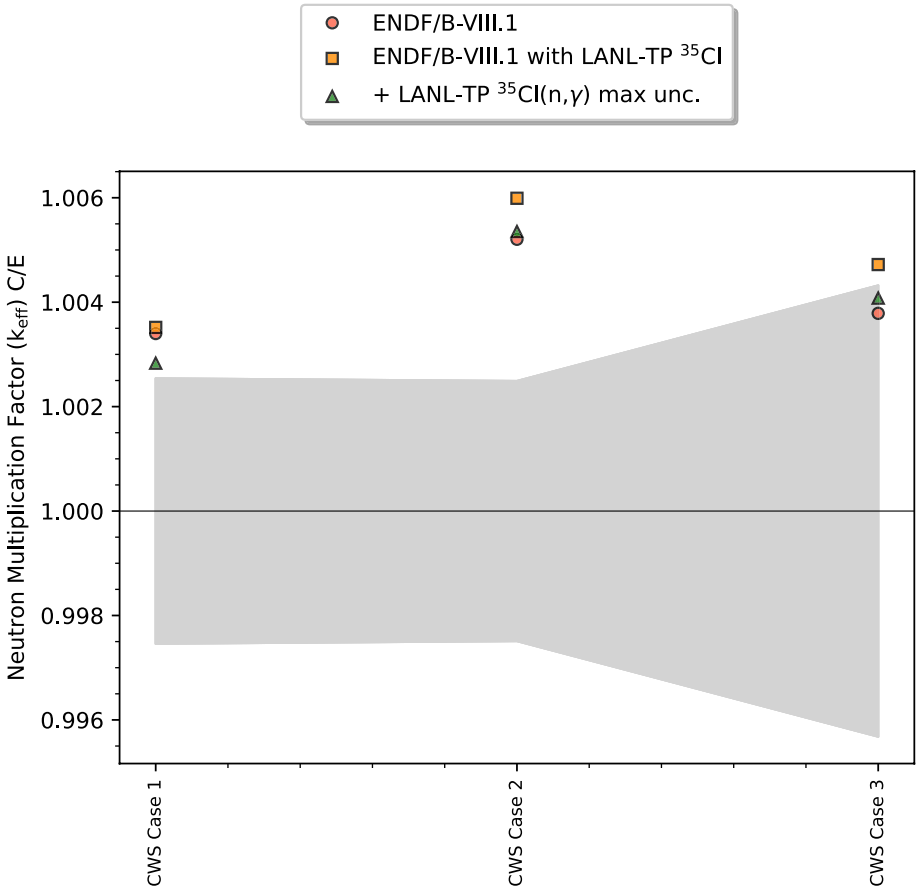

Fig. 7. Calculated-to-experimental ratios of k_{eff} values for various cases of the CWS [16], calculated under varying nuclear data. The measured values are represented by the gray uncertainty band while calculations are shown as individual markers. In comparison are the results using the ENDF/B-VIII.1 library (circles), the same with LANL-TP substituted for ^{35}Cl (squares), and the effect of perturbing the LANL-TP ^{35}Cl(n,γ) cross section by the maximum of its evaluated uncertainty per energy group (triangles).

Figure 7 shows the results for the full ENDF/B-VIII.1 library with LANL-TP replaced for ^{35}Cl, and the same if the capture cross section for ^{35}Cl is increased to the maximum limit of the evaluated uncertainty, i.e. $+1\sigma$ per energy group. The measured results from the CWS are represented by the gray uncertainty band around C/E = 1. In all cases, this increase in neutron absorption due to capture on chlorine does bring the results back to closer agreement with the measurements; however, only in Case 3 is this agreement within a standard deviation. As expected for the CWS, energy group sensitivity analysis indicates that this change comes about overwhelmingly through the thermal region, specifically from thermal up to 0.1 keV, where the evaluated uncertainty is quoted as being a flat 1.2%. Larger adjustments, outside the previously evaluated uncertainties, to the (n, γ) cross section could be made to improve the comparison. However, γ-production from the ^{35}Cl(n,γ) reaction is often used as a reference standard for calibrating γ-ray detectors [26], hence a careful re-evaluation of the chlorine nuclear data in the Resolved Resonance Region (RRR) down to thermal is required to identify whether the current discrepancies are due to chlorine or if improvements need to be made elsewhere.

Even so, the validation of the LANL-TP fast evaluation allows us to start drawing some conclusions about potential shortfalls in the current chlorine evaluation at lower neutron energies than those studied in this work. In the R-matrix analysis of Sayer et al. [27], which formed the current ENDF/B evaluation in the RRR from thermal to approximately 1.2 MeV, the thermal cross sections are consistent with the evaluation of Mughabghab et al. [28], with adopted uncertainties around 1.2%. In the years since, it has been noted by multiple studies [29–32] that the average (n,γ) cross sections from the ENDF/B evaluations show significant discrepancies, altogether suggesting an increase on the order of ∼15% between the thermal and epithermal regions. This adjustment is well outside the uncertainty of the Mughabghab evaluation for thermal, but within the uncertainty bounds of the RRR (about 10–15% maximum on average), highlighting the need to re-evaluate the chlorine cross sections down into the thermal and epithermal energy ranges.

Future benchmarks promise to provide even greater sensitivity in the regions of interest. This includes the recent TEX-Cl experiment [17] performed at the National Criticality Experiment Research Center (NCERC). As discussed in the TEX-Cl design report, the designs involve two configurations that are more sensitive to capture on chlorine at thermal energies, complementary to the CWS, and one case that is more sensitive to fast energies and is relevant for certain upset cases in the operation of the MCRE. Even faster configurations are currently

being designed [33] to be measured at NCERC that will be even more compatible with the operating conditions of the MCRE. Therefore, while a fuller sensitivity study of the available benchmark data is beyond the scope of this work, there are plans to return to this study in more detail together with the future TEX-Cl benchmark results to help elucidate the broader impacts of our improved constraints on the chlorine nuclear data.

Conclusion and outlook

We have tested and validated the recently published LANL-TP evaluation of the fast-energy ^{35}Cl cross sections against ENDF/B-VIII.1 through simulation and measurement of the ^{252}Cf(s.f.) spectrum average cross sections of ^{35}Cl(n,p_0) and ^{35}Cl(n,p+n,α). Comparisons of the ratios of calculated to experimental values show that LANL-TP brings the SACS within a standard deviation of expected values, while results for ENDF/B-VIII.1 remain notably more discrepant. Preliminary comparisons to the Chlorine Worth Study benchmark indicate that the new fast evaluation cannot resolve the existing discrepancies between calculated and experimental k_{eff} values in that study, as it is mostly sensitive to thermal neutron energies. Future benchmarks such as TEX-Cl will open up greater sensitivity to the fast and epithermal energy ranges, benefiting from the stringent constraints at fast energies provided from this work.

Having well constrained the fast-energy region in this and previous works, new measurements are underway at LANL to constrain the resonance parameters of the (n,p) reaction cross section at lower energies using isotopically enriched ^{35}Cl targets. New measurements of transmission and neutron capture with isotopically enriched targets are also feasible at LANSCE using the DICER [34] and DANCE [35] detector arrays, which are complementary to the (n,p) measurements. These measurements are important for improving the evaluations, together with the ongoing criticality benchmarks, for Nuclear Criticality Safety applications. However, the impact of this current work fundamentally improves the confidence on the use of the LANL-TP chlorine nuclear data evaluation, compared to other available evaluations, for simulations of the MCRE operation.

Data availability

The evaluated nuclear data file (LANL-TP) in ENDF6 format and the corresponding data processed into GEANT4 NDL and MCNP ACE input files are available upon request to K.H., the corresponding author.

Received: 21 July 2025; Accepted: 10 November 2025
Published online: 03 December 2025

References

1. Nuclear Energy Agency. *NEA Nuclear Data High Priority Request List*. https://www.oecd-nea.org/dbdata/hprl/.
2. Cutler, T., Amundson, K., Hutchinson, J., Kleedtke, N. & Wynne, N. The CWS experiments – An experimental study of the effects of chlorine on thermal neutron absorption. In *Proceedings: Nuclear Criticality Safety Division Topical Meeting (NCSD 2022)*. 276–285 (2022). https://doi.org/10.13182/T126-37503.
3. Hanselman, K. et al. *Phys. Rev. C* **110**, 024609. https://doi.org/10.1103/PhysRevC.110.024609 (2024).
4. Rising, M. E. et al. MCNP® Code Version 6.3.0 Release Notes. In Technical Reports LA-UR-22-33103, Rev. 1, Los Alamos National Laboratory, Los Alamos, NM, USA (2023). https://www.osti.gov/biblio/1909545.
5. Agostinelli, S. et al. Geant4—A simulation toolkit. *Nucl. Instrum. Methods Phys. Res. Sect. A Accel. Spectrom. Detect. Assoc. Equip.* **506**, 250–303 (2003). https://www.sciencedirect.com/science/article/pii/S0168900203013688.
6. Allison, J. et al. Geant4 developments and applications. *IEEE Trans. Nucl. Sci.* **53**, 270–278 (2006).
7. Allison, J. et al. Recent developments in Geant4. *Nucl. Instrum. Methods Phys. Res. Sect. A Accel. Spectrom. Detect. Assoc. Equip.* **835**, 186–225 (2016). https://www.sciencedirect.com/science/article/pii/S0168900216306957.
8. Cisneros, T. et al. Reactivity impact of updated 35Cl nuclear data on the molten chloride reactor experiment. *Nucl. Sci. Eng.* 1–11. https://doi.org/10.1080/00295639.2024.2413787 (2024).
9. Smith, M. B. et al. Fast neutron measurements using cs2liycl6:ce (clyc) scintillator. *Nucl. Instrum. Methods Phys. Res. Sect. A Accel. Spectrom. Detect. Assoc. Equip.* **784**, 162–167 (2015). https://www.sciencedirect.com/science/article/pii/S0168900214010225 [Symposium on Radiation Measurements and Applications 2014 (SORMA XV)].
10. Recker, M. C. *Enabling Mobile Neutron Detection Systems with CLYC*. Ph.D. Thesis, Department of the Air Force, Air University, Air Force Institute of Technology (2019).
11. Ferrulli, F., Labalme, M. & Silari, M. Investigation of CLYC-6 for thermal neutron detection and CLYC-7 for fast neutron spectrometry. *Nucl. Instrum. Methods Phys. Res. Sect. A Accel. Spectrom. Detect. Assoc. Equip.* **1029**, 166460 (2022). https://www.sciencedirect.com/science/article/pii/S0168900222000973.
12. Kelly, K. J. et al. Measurement of the cross section of the $q = 4.4398$ mev $^{12}\mathrm{C}(\mathrm{n,n'}\gamma)$ reaction from threshold to 16.5 mev using γ and correlated n- γ detection. *Phys. Rev. C* **108**, 014603 (2023). https://doi.org/10.1103/PhysRevC.108.014603.
13. Kelly, K. J., Bennett, E. A., Devlin, M., O'Donnell, J. M. & Paris, M. The neutron scattering cross section and angular distribution measurement program at lanl. *EPJ Web Conf.* **284**, 01004. https://doi.org/10.1051/epjconf/202328401004 (2023).
14. Mannhart, W. Status of the Cf-252 fission neutron spectrum evaluation with regard to recent experiments. In *INDC(NDS)-220/L*. Vol. 305 (1989).
15. Koning, A. J. et al. TENDL: Complete nuclear data library for innovative nuclear science and technology. *Nucl. Data Sheets* **155**, 1–55 (2019). https://www.sciencedirect.com/science/article/pii/S009037521930002X (special issue on nuclear reaction data).
16. Thompson, N. W. et al. Chlorine Worth Study Nuclear Data (Los Alamos National Laboratory (LANL), Los Alamos, NM (United States), 2024). https://www.osti.gov/biblio/2345728.
17. Aboud, E. et al. Final design for thermal/epithermal eXperiments (TEX) with chloride absorbers to provide validation benchmarks for Y-12 electrorefining facility. In Technical Report, Lawrence Livermore National Laboratory (LLNL), Livermore, CA (United States) (2023). https://www.osti.gov/biblio/2202542.
18. Kirsch, L. E., Devlin, M., Mosby, S. M. & Gomez, J. A. *Nucl. Instrum. Meth. Phys. Res. A* **874**, 57–65 (2017) https://www.sciencedirect.com/science/article/pii/S0168900217309464.
19. Mattera, A., Zhu, S., Hayes, A. & Mccutchan, E. *Nuclear Data Sheets* **172**, 543–587 (2021) https://www.sciencedirect.com/science/article/pii/S0090375221000028.
20. Kahler III, A. C. & Macfarlane, R. Njoy2016 (2016). https://www.osti.gov/biblio/1339450.
21. Mendoza, E. & Cano-Ott, D. Update of the evaluated neutron cross section libraries for the geant4 code. *IAEA Technical Report INDC(NDS)-0758, Vienna, 2018* (2018).

22. PNNL. Compendium of material composition data for radiation transport modeling. In *200-DMAMC-128170 PNNL-15870, Rev. 2* (2021).
23. Kuvin, S. A. et al. Validation of neutron-induced reactions on natural carbon using an active target at neutron energies up to 22 MeV at lansce. *Phys. Rev. C* **104**, 014603. https://doi.org/10.1103/PhysRevC.104.014603 (2021).
24. Kleedtke, N., Haeck, W. & Hutchinson, J. Utilization of ace nuclear data file toolkit acetk to calculate relative sensitivity coefficients of point-kinetics parameters. *Ann. Nucl. Energy* **193**, 110031 (2023) https://www.sciencedirect.com/science/article/pii/S03064549 2300350X.
25. Nuclear Energy Agency (ed.) *International Handbook of Evaluated Criticality Safety Benchmark Experiments* (OECD Nuclear Energy Agency, 2021).
26. Molnár, G. L., Révay, Z. & Belgya, T. Accurate absolute intensities for the 35cl(n,γ) reaction gamma-ray standard. *Nucl. Instrum. Methods Phys. Res. Sect. B Beam Interact. Mater. At.* **213**, 32–35 (2004). https://www.sciencedirect.com/science/article/pii/S01685 83X03015295 (5th Topical Meeting on Industrial Radiation and Radioisotope Measurement Applications).
27. Sayer, R. O., Guber, K. H., Leal, L. C., Larson, N. M. & Rauscher, T. R-matrix analysis of Cl neutron cross sections up to 1.2 MeV. *Phys. Rev. C* **73**, 044603 (2006). https://doi.org/10.1103/PhysRevC.73.044603.
28. Mughabghab, S. F., Divadeenam, M. & Holden, N. E. *Neutron Cross Sections*. Vol. 1 (Academic Press, 1981).
29. Pavetich, S. et al. Accelerator mass spectrometry measurement of the reaction $^{35}\mathrm{Cl}(n,\gamma)^{36}\mathrm{Cl}$ at kev energies. *Phys. Rev. C* **99**, 015801 (2019). https://doi.org/10.1103/PhysRevC.99.015801.
30. Macklin, R. L. Resonance neutron capture by $^{35,37}\mathrm{Cl}$. *Phys. Rev. C* **29**, 1996–2000. https://doi.org/10.1103/PhysRevC.29.1996 (1984).
31. Guber, K. H. et al. New maxwellian averaged neutron capture cross sections for $^{35,37}\mathrm{Cl}$. *Phys. Rev. C* **65**, 058801. https://doi.org/ 10.1103/PhysRevC.65.058801 (2002).
32. Bennett, S. A. Measurements of the ^{13}C and ^{35}Cl radiative neutron capture reaction cross sections. Ph.D. Thesis, Department of Physics and Astronomy in the School of Natural Sciences, The University of Manchester (2021).
33. Branco-Katcher, M. et al. Design optimization of a criticality experiment for the molten chloride reactor experiment facility. *Nucl. Sci. Eng.* 1–22. https://doi.org/10.1080/00295639.2025.2464459 (2025).
34. Stamatopoulos, A. et al. New capability for neutron transmission measurements at lansce: The dicer instrument. *Nucl. Instrum. Methods Phys. Res. Sect. A Acc. Spectrom. Detect. Assoc. Equip.* **1025**, 166166 (2022). https://www.sciencedirect.com/science/articl e/pii/S0168900221010457.
35. Heil, M. et al. A 4πbaf2 detector for (n,γ) cross-section measurements at a spallation neutron source. *Nucl. Inst. Methods A* **459**, 229–246 (2001) https://www.sciencedirect.com/science/article/pii/S0168900200009931.

Acknowledgements

This work was carried out under the auspices of the National Nuclear Security Administration of the US Department of Energy at Los Alamos National Laboratory under Contract No. 89233218CNA000001. We would like to thank Drs. Keegan Kelly, Patrick Copp, and the CoGNAC experimental group at LANSCE for the use of their spare CLYC detectors and expertise. We would also like to thank M. Espy, A. Escobedo, and V. Gurrola of LANL's Nondestructive Testing and Evaluation group for performing the CT scans of the C7LYC detector. Finally, we acknowledge Emilio Mendoza from CIEMAT for assistance in processing the LANL-TP evaluation file into a GEANT4 NDL input file.

Author contributions

S.A.K. and K.H. conceived the experiment. I.J.A., S.A.K., K.H., and S.N.P. analyzed the experimental data and developed the GEANT4/MCNP simulations. J.W. provided equipment and assistance during the measurements. N.K. and K.H. performed the Chlorine Worth Study comparisons with consultation with S.A.K. and N.T. MCRE discussions were assisted by T.C., B.H., and M.W. T.K. and H.Y.L. provided guidance on nuclear data evaluation and measurements and additional oversight. All authors reviewed the manuscript.

Funding

This project was supported by the DOE Office of Science Undergraduate Laboratory Internships (SULI) program; the Nuclear Criticality Safety Program, funded and managed by the National Nuclear Security Administration for the Department of Energy; the Laboratory Directed Research and Development program of LANL under Project No. 20230534ECR; and the US Nuclear Data Program under the DOE Office of Science – Office of Nuclear Physics. The Chlorine Worth Study was funded under the Material Recycle and Recovery Program, NNSA Plutonium Program Office (NA-191), under Office of Production Modernization (NA-19), funded and managed by the National Nuclear Security Administration for the Department of Energy. Production of the LANL-TP evaluated nuclear data was funded by the U.S. Department of Energy Office of Nuclear Energy/Gateway for Accelerated Innovation in Nuclear (GAIN) voucher NE-22-28590 and a Cooperative Research and Development Agreement (CRADA) with TerraPower LLC.

Declarations

Competing interests

The authors declare no competing interests.

Additional information

Correspondence and requests for materials should be addressed to K.H.

Reprints and permissions information is available at www.nature.com/reprints.

Publisher's note Springer Nature remains neutral with regard to jurisdictional claims in published maps and institutional affiliations.